

## **Influence of the Subarachnoidal Cerebrospinal Fluid Layer on the Dynamic Response of the Brain: An Experimental and Computational Study**

F. A. Bandak, P. C. Chan, J. Yu, and J. Stuhmiller

### **ABSTRACT**

*The brain and cranium are separated by a thin layer of cerebrospinal fluid (CSF) that plays an important role in the brain response under impact loading. Understanding the pressure response of the CSF layer is an important first step in the characterization of the brain response under impact conditions. Under severe impact, the fluid pressure can drop below its vapor pressure and cavitation bubbles, which have been postulated to cause contrecoup damage, can form. This paper describes an experimental and computational fluid dynamics study using idealized physical and computational models of the brain-cranium system to investigate 1) effects of variations in the gross mechanical properties of the brain and 2) influence of flow out of the foramen magnum. Indication of coup as well as contrecoup cavitation was observed, resulting in large, violent pressures during the collapse phase that may well be associated with brain injury.*

### **INTRODUCTION**

**M**otor vehicle crashes can result in occupant impacts that subject the head to structural deformation as well as acceleration effects that can cause the brain to move within the cranial cavity. Such movements can result in cerebrospinal fluid pressures that affect the pressure gradients within the brain itself. If such gradients contain sudden drops reaching negative pressure values of one atmosphere, the brain parenchyma may experience local damage including vascular ruptures (Unterharnscheidt and Ripperger, 1970).

Physical model studies have been used to investigate brain response related to injury mechanisms. Ljung (1975) used physical models to study brain motion resulting from pure rotation. He showed that significant brain motion relative to the interior surface of the cranium occurs. Pure translational head acceleration, however, results in limited motion of the brain that is generally translational. The associated CSF response under such motion has not been characterized. Impact accelerations induce strong pressure

gradients in the mature brain with positive and negative values (Denny-Brown and Russell, 1941). Gross (1958) postulated that cavitation would also occur if the contrecoup pressure drops below the water vapor pressure, and the subsequent collapse of cavitation bubbles might cause serious brain injuries. These injuries have been observed to occur on the side of the head opposite to the impact site and have been labeled as contrecoup injuries. Although contrecoup injuries have been accepted clinically (Unterharnscheidt and Ripperger, 1970; Stalhammar, 1970), debate about their mechanisms still exists. Computational and experimental results (Kopecky and Ripperger, 1969) have demonstrated that an acceleration of about 150g can produce negative pressures with magnitudes sufficient to cause cavitation.

Several experimental studies have been conducted using biological models to try to obtain realistic data. These included primate tests (McElhaney et al., 1973), embalmed cadavers (Ward, 1983; Viano et al., 1989), or data from clinical reports and eyewitness interviews on motor vehicle crash head injury (Mohan et al., 1979). Idealized physical models can be effectively used to study specific phenomena, since they simplify the analysis and reduce the uncertainty in data interpretation. Kenner and Goldsmith (1973) impacted water-filled spherical shells of various sizes to produce loadings with different magnitude and duration. They compared pressure distributions and shell strain measurements with analytical results.

The purpose this study is to investigate, experimentally and computationally, the fundamental fluid dynamic response of the CSF layer surrounding the brain. The quantitative understanding of the fluid dynamics behaviour of the CSF layer will provide insight into the operative mechanisms that may be responsible for injury as well as insight for modelling the interface between the cranium and the brain.

## METHODS

### Experimental

An idealized physical model of the cranium-brain was developed and used to study internal pressure response under various impact loadings (Fig. 1). The cranium was made of two 8 in., hollow, Plexiglas hemispheres bolted together at an equatorial flange. A 2 in. opening at the top (polar cap) of the model was made to install a fiber-reinforced diaphragm for load application. The diaphragm was used to induce more local deformation than can be produced by impacting the Plexiglas directly. The brain was simulated using a balloon filled with various materials. Water was used to simulate the subarachnoidal CSF in the gap between the cranium and the balloon. Before each test, a metered amount of water was placed inside the cranium, and then a balloon was inserted into the cranium through a discharge port located at 112.5° from the polar cap (Fig. 2). A rubber stopper was used to wedge the neck of the balloon in place before it was pressure filled with the desired material. A small tube connected to an adjustable water column through the rubber stopper was used to regulate the flow in and out of the balloon to simulate the effect of the foramen magnum (Fig. 2). Pressure gauges P1, P2, P3 and P4 were located at four polar locations of 45°, 135°, 180°, and 225° on the same vertical plane (Fig. 1). The gauges were PCB piezoelectric transducers (model 113M182) tapped into the Plexiglas shell. The gauge outputs were fed to a four channel Nicolet Model 4094 digital memory scope for direct display and later transferred to a desktop computer for analysis.

Two test configurations that attempted to isolate the effects of deformation and acceleration were considered. In the deformation-impact tests, the model was rigidly held in place, so that there was no whole-head acceleration resulting from impact against the top flexible diaphragm producing controlled local deformation. A controlled drop of a weight onto the neoprene diaphragm (Fig. 2) generated the impact. The pulley arrangement guaranteed that the drop height could be consistently controlled and that the impact point was always centered on the diaphragm.

In the acceleration-impact tests, the model was allowed to swing freely and the impact was delivered to the nearly rigid equatorial flange. Analysis of the impact experiments revealed that some deformation

occurred in the sphere model. A second model used a delrin insert, with the same internal diameter as the sphere and 0.5 in. larger in outer radius than the flange, sandwiched between the two hemispheres to receive the impact. The model was allowed to swing freely after pendulum impact on the equatorial plane. The pendulum impact mechanism is shown in Figure 3.

Two types of strikers were used for this series of tests. A 2.5 in. diameter, 1.25 in. thick brass disk that weighs 1 lb. 15.5 oz was used for the direct impact tests. A vertical board was used to guide the movement of the disk along the plane so that it hits the flange of the model directly and transmits the load to the model surface. The second striker was a 3.0-in. diameter titanium sphere threaded at the end of a 0.5-in. diameter 3-ft long steel rod. The rod was mounted to a linear bearing that allows the sphere to swing only in the plane parallel to the mounting surface. The pendulum, including the rod, weighs 9 lb. 13.2 oz.

## Computational

The fluid computations were conducted using the Eulerian two-fluid transport equations with heat and mass transfer. The analysis assumed that the liquid and gas phases are dispersed locally so that the mixture equations of motion can be used. The governing equations in cylindrical coordinates are as follows.

### Conservation of mass (liquid)

$$\frac{\partial(m_L)}{\partial t} + \frac{1}{r} \frac{\partial(r m_L u)}{\partial r} + \frac{1}{r} \frac{\partial(m_L v)}{\partial \theta} + \frac{\partial(m_L w)}{\partial z} = -\Gamma \quad (1)$$

### Conservation of mass (gas)

$$\frac{\partial(m_G)}{\partial t} + \frac{1}{r} \frac{\partial(r m_G u)}{\partial r} + \frac{1}{r} \frac{\partial(m_G v)}{\partial \theta} + \frac{\partial(m_G w)}{\partial z} = \Gamma \quad (2)$$

### Equations of Motion

$$\frac{\partial u}{\partial t} + u \frac{\partial u}{\partial r} + \frac{v}{r} \frac{\partial u}{\partial \theta} + w \frac{\partial u}{\partial z} - \frac{v^2}{r} = -M \frac{1}{m_L + m_G} \frac{\partial p}{\partial r} + g_r + \left( \frac{\alpha_L \mu_L + \alpha_G \mu_G}{m_L + m_G} \right) \nabla^2 u \quad (3)$$

$$\frac{\partial v}{\partial t} + u \frac{\partial v}{\partial r} + \frac{v}{r} \frac{\partial v}{\partial \theta} + w \frac{\partial v}{\partial z} + \frac{uv}{r} = -\frac{1}{m_L + m_G} \frac{1}{r} \frac{\partial p}{\partial \theta} + g_\theta + \left( \frac{\alpha_L \mu_L + \alpha_G \mu_G}{m_L + m_G} \right) \nabla^2 v \quad (4)$$

$$\frac{\partial w}{\partial t} + u \frac{\partial w}{\partial r} + \frac{v}{r} \frac{\partial w}{\partial \theta} + w \frac{\partial w}{\partial z} = -\frac{1}{m_L + m_G} \frac{\partial p}{\partial z} + g_z + \left( \frac{\alpha_L \mu_L + \alpha_G \mu_G}{m_L + m_G} \right) \nabla^2 w \quad (5)$$

### Equations of State

$$\rho_L = \rho_L^o + \frac{1}{c_L^2} (p - p^o) \quad (6)$$

$$\rho_G = \rho_G^o \left( \frac{p}{p^o} \right)^\gamma \quad (7)$$

### Conservation of volume

$$\frac{m_L}{\rho_L} + \frac{m_G}{\rho_G} = 1 \quad (8)$$

With  $t$  as time,  $u$ ,  $v$  and  $w$  are the three velocity components in the radial, azimuthal and axial coordinates,  $r$ ,  $\theta$  and  $z$ , respectively. The boiling rate,  $\Gamma$ , models the interfacial mass transfer,  $\rho_L$  and  $\rho_G$  represent the

liquid and gas material densities,  $m_l$  and  $m_g$  are their bulk densities, respectively, and  $\alpha_l$  and  $\alpha_g$  are the liquid and gas volume fractions. The pressure is  $p$ , and  $g_r, g_\theta$ , and  $g_z$  are the three external body acceleration components (Eqs. 3-5). Since fluid velocities are expected to be low and compressibility effect is small, the fluid stress terms are approximated as diffusion terms where  $\mu_l$  and  $\mu_g$  are the dynamic viscosities of liquid and gas, respectively. Both the liquid and gas phases are compressible. The liquid compressibility is modelled with a constant sound speed,  $c_l$ , where the superscript 0 refers to a reference state (Eq. 6). For a low speed adiabatic process without shock waves, the gas phase can be assumed to follow an isentropic expansion with a constant specific heat ratio,  $\gamma$ , (Eq. 7).

A dynamic flow-regime boiling model (Chan, Masiello, and Srikantiah, 1986) simulated cavitation. The boiling rate,  $\Gamma$ , (mass/volume/time) is

$$\Gamma = \frac{3fk\alpha_l\alpha_g}{r_b^2 h_{fg}} (T_l - T_s) \quad (9)$$

where  $f$  is a constant,  $r_b$  is the mean bubble radius,  $k$  is the liquid heat conductivity,  $h_{fg}$  is the latent heat of vaporization,  $T_l$  is the liquid temperature, and  $T_s$  is the saturation temperature. The liquid temperature  $T_l$  is kept constant at the laboratory ambient value, 70 °F, but the saturation temperature  $T_s$  varies with pressure. Thus boiling or condensation occurs when  $T_s$  is lower or higher than  $T_l$  respectively.

The system of partial differential equations was solved by finite difference. In the computational domain, staggered meshes were used where scalars like the pressure and density were placed at cell centers, and velocities were placed at and normal to cell faces, as illustrated in Figure 4 for the  $r-\theta$  plane. The governing equations were recast into a system of difference equations according to the semi-implicit algorithm of Liles and Reed (1978). Although the equations were integrated from time level  $n$  to  $n+1$  explicitly, a robust coupling between velocity and pressure is preserved by taking the velocities in the continuity equations (Eqs. 1-2) and the pressure in the momentum equations (Eqs. 3-5) always at the new time level  $n+1$ . By a series of Gaussian eliminations, a system of difference equations for the pressure is obtained for the entire computational domain, which is solved by an alternating direction line successive over-relaxation (LSOR) method. Once the pressure is known, all the other dependent variables can be obtained by back substitution. Details of this methodology are available from several sources (Chan and Klein, 1994; Chan, Masiello and Srikantiah, 1986; Klein, Chan and Chan, 1989; Chan and Klein, 1989).

A planar two-dimensional (cylindrical) model representing the cross-section of the spherical physical model was used for the computational study. An outer cylinder with 8-in. diameter was to represent the cranium with a 7.3-in. diameter brain is located concentrically inside (Fig. 5). A layer of cerebrospinal fluid is placed between the cranium and the brain. The brain and the CSF were modelled as two distinct fluids with a sharp interface. An interface-sharpening algorithm was used to remove the effects of numerical diffusion and preserve the CSF-brain interface. Twenty fine radial cells were clustered in the CSF layer, and the brain region was resolved with 20 nonuniform radial cells. There were 36 uniform azimuthal cells. Distinct material properties were prescribed for the CSF and the brain. The brain density was taken as 71.76 lb/ft<sup>3</sup>, which is to be 15% heavier than the CSF (Engin and Liu, 1970). The brain kinematic viscosity was estimated to be 0.097 ft<sup>2</sup>/s (Ljung, 1975), which is 10,000 times that of water. The CSF was taken to have the same density and viscosity as water. Calculations were also performed with the brain density and viscosity the same as the CSF. The sound speed of the liquid phase was taken to be 5000 ft/sec. Acceleration and cranial deformation were applied for simulation. The acceleration,  $a(t)$ , followed a sinusoidal function

$$a(t) = A \sin\left(\frac{\pi t}{T}\right) \quad (10)$$

where  $A$  is the peak value, and  $T$  is the pulse duration (Hosey and Liu, 1982). A rigid cranium was modelled by prescribing zero normal fluid velocity at the boundary cells. Cranial deformation was simulated by imposing inflow velocity at selected boundary cells. To model cranium indentation and snap back at the impact site, a normal flow velocity following the acceleration curve (Eq. 10), with selected  $A$  and  $T$ , is prescribed at a number of boundary cells centered at the pole site. No slip tangential fluid velocity is imposed at the cylinder boundary.

## RESULTS

### Experimental

The repeatability of the deformation impact tests was confirmed for each configuration. An example is shown for the configuration where the balloon was filled with water and the discharge port was closed. The test was repeated four times and the overlaid pressure traces are shown in Figure 6. Not only are the peak pressures and durations replicated, but also many of the fine details of the pressure variation, probably due to the flexure of the cranium model and the impact diaphragm are seen in each trace. The experimental procedure was judged to be sensitive enough to distinguish small variations caused by changes in the test configuration.

The effects of the flow through the opening simulating the "foramen magnum" indicate that as the exit pressure water column is reduced, the flow out of the balloon is increased and the internal pressure is relieved (Fig. 7). For the conditions tested, the outflow reduces the peak pressure and total duration of the positive phase by about 10%. The exit flow area may not represent correctly the actual foramen magnum and, therefore, the pressure relief effects may be greater or lesser.

The main factor affecting the pressure response was the difference in brain simulant materials. Four simulant cases were considered: 1) a water filled balloon (base case); 2) a gelatin-filled balloon; 3) a water-filled balloon with a 2.5 in. diameter air balloon in it (overall void volume fraction of 3.1%); and 4) a rigid Plexiglas sphere. The pressure response for these cases at location P1 under the condition of a closed exit is shown in Figure 8. The response of the solid and water-filled balloon was nearly identical. The gelatin-filled model showed a faster reduction of pressure following the peak which may be an indication of direct interaction between the diaphragm and the balloon (Fig. 8).

The case where the brain simulant was a water filled balloon with a 3.1% volume fraction of air showed the most significant effects on pressure response (Fig. 8). The relatively small volume of air contributed to a nearly 50% reduction in peak pressure and the generation of higher frequency pressure fluctuations. The compressibility of the air bubble resulted in a different internal flow pattern as indicated by pressure oscillations that were out of phase with one another.

The pendulum acceleration-impact tests showed that the sphere model has good repeatability. In these tests, the pressure gauges on the impact side (P1 and P2) are referred to as the coup side, the gauge on the opposite side (P4) as the contrecoup side, and P3 as the mid-plane. The pressure response to strong acceleration (Figure 9) indicates that the acceleration phase lasted about 0.5 ms during which the coup side experienced an overpressure of 40-50 psig, while the contrecoup side experienced a pressure drop to the limit of -14.7 psig indicating that cavitation probably occurred. At the end of the acceleration period, the contrecoup pressure shows a pressure increase (within a few hundredths of a millisecond) of about two atmospheres (Fig. 9). This rapid increase is characteristic of a cavitation bubble collapse.

Following acceleration, the coup side pressure continues to drop below ambient and levels off near absolute zero, a strong indication that cavitation has occurred on the coup side (Fig. 9). The cause of the cavitation state that is maintained for about 0.5ms is probably the “snap back” of the local deformation of the sphere. The results indicate that this collapse event results in an overpressure spike that is quite energetic reaching 100-120 psig. Figure 10 shows the pressure response on the coup and contrecoup sides for impacts which are above and below the level at which cavitation occurs. At low acceleration, the pressures oscillate in time and are out of phase, as would be expected, on the two sides. At no time did the pressures approach absolute zero. The character of the pressure variation dramatically as evidenced by the cavitation collapse spikes. These results suggest that there is a critical level of impact-induced, whole-head, acceleration and duration at which cavitation occurs.

The accelerometer at the “north pole” of the spherical model provided an estimate of the acceleration resulting from impacting the delrin-reinforced sphere with a titanium impactor. The initial acceleration pulse lasted about 1.5 msec and the peak increased from about 50 g’s to about 200 g’s as the pendulum height was raised. The erratic behaviour of the acceleration following the initial impact is believed to be due to structural vibration since it contributes little to the velocity (Fig. 11). The pressure response increases, as expected, with the strength of the impact acceleration pulse (Fig.12). The coup side pressure (P2) has a peak that ranges from 8 to 25 psi. The reduced deformation of the sphere results in a reduced snap back effect and so no coup-side cavitation is observed (Fig. 12a). The contrecoup side (P4) indicates the opposite; the peak pressure reaching higher negative values as expected with increasing acceleration (Fig. 12b). At the greatest pendulum heights, the pressure reached cavitation levels, followed by very rapid pressure increases, again characteristic of bubble collapse. The high pressures from the collapse are propagated across the model and show up as a second pressure peak on the coup side at around 2.8ms (Fig. 12).

## Computational

Calculations were performed to study three fluid dynamics effects due to head impact: 1) brain and CSF motion, 2) brain pressure response due to cranial deformation and acceleration, and 3) cavitation and bubble collapse. Calculated results for the latter two studies were compared to selected experimental results.

In a baseline calculation using a rigid cranium, with the brain and CSF having the same density and viscosity and not allowed to cavitate, the model was subjected to acceleration loading with 150-g peak and 4 ms duration. The coup and contrecoup pressures were symmetric about the midplane (Fig. 13). With brain-CSF density ratio being 1, no CSF or brain movement was observed. The pressure difference across the brain increases with acceleration and reaches the maximum peak values of  $\pm 21.5$  psi at 2 ms. The contrecoup pressure drops below the vapor pressure at 0.9 ms, and cavitation can occur. Fluid motion developed when the baseline calculation was repeated with the brain density and kinematic viscosity taken as 71.76 lb/ft<sup>3</sup> and 0.097 ft<sup>2</sup>/s, respectively (Fig. 14). Acceleration causes the brain to move forward and squeeze the CSF fluid backward with velocity reaching 1.6 ft/s. The brain motion increases the coup compression and the contrecoup tension. The heavier brain (15%) increases the peak pressure gradient across the brain by about 16%. With a heavier brain, the peak coup pressure increases by 24% to 26 psig when compared to the baseline case (Fig. 13). However, the contrecoup pressure only reduces by 7% to -23 psig at 2 ms. This uneven coup-contrecoup pressure change may be partially due to the CSF flow effect. **Since the brain moves forward, the CSF has to flow backward, but it must also stagnate at the antipole and may prevent the pressure to drop proportionally to the coup pressure increase.** Similar brain motion was observed when the calculation, with distinct CSF and brain properties, was repeated with a 2 ms acceleration pulse, while keeping peak acceleration at 150 g. Other than the pulse duration being shorter, the asymmetric coup-contrecoup pressure pattern is similar to that of the long pulse (Fig. 13).

The normalized relative displacement produced by both the short and long pulses rise steadily to 0.031 and 0.067, respectively, at 12 ms (Fig. 15), suggesting that the brain can move by a few percent of the CSF gap under these accelerations. The relative displacement between the brain and the cranium was estimated by an inferred strain,  $\varepsilon$ , given by

$$\varepsilon = \int_0^t \frac{v}{\delta} dt \quad (11)$$

where  $v$  is the azimuthal fluid velocity at the brain surface, and  $\delta$  is the width of the CSF layer.

The analysis of combined effects of cranial deformation and acceleration on intracranial pressures was compared with the experiment that used water enclosed by the spherical shell. The calculation was made with the density and viscosity of both the brain and CSF set equal to water and the model was subjected an acceleration with 1 ms duration, as suggested by the data (Eq. 10). The calculation was repeated with the brain having higher density and viscosity values. The structural deformation was imposed as a sinusoidal velocity inflow condition at the cranium boundary over a  $20^\circ$  segment centered at the pole with a peak of -1 ft/s, which corresponds to a deformation of about 0.006 in. over 1 ms (Fig. 5a). As in the experiment, CSF pressures at four locations were monitored, as shown in Figure 5a, with P1 and P2 on the coup side, P3 on the midplane, and P4 on the contrecoup side.

Simulations show that structural deformation increases the coup-contrecoup pressure peak magnitudes significantly and in an asymmetric manner. For the case with the brain and CSF having the same density and viscosity as water, the frontal cranial deformation increases the peak pressure magnitudes by at least 20%, when compared to the rigid cranium model (Fig. 16a). When distinct brain and CSF properties are used, the coup peak pressure is further increased to almost twice the value for the rigid cranium (Fig. 16a). The indentation of the impact region causes the coup pressure at P1 to rise faster than the contrecoup pressure drop at P4. Near the end of the pulse at about 0.8 ms, the structural snap back of the impact site creates a fluid tension, causing P1 to drop below zero (Fig. 16a).

Using the model with the brain and CSF having water properties as in the experiment, the calculated pressures at P1 and P4 with cranial deformation compare favourably with data (Fig. 16a), including the peaks and timing (Fig. 16). Compared to the calculation, the data show a stronger snap back effect near the end of the acceleration, with the coup pressure (P1) dropping lower and the contrecoup pressure (P4) recovering earlier. The recorded oscillations beyond 1 ms probably came from the Plexiglas structural ringing excited by the loading and was not modelled.

The effect of CSF cavitation caused by acceleration and snap back of the frontal impact site was simulated using a model with the brain and CSF having water properties similar to the test model. An acceleration pulse with 150-g peak and 0.5 ms duration was imposed, as suggested by test data. To simulate the structural snap back on the coup side, a sinusoidal outflow with 2 ft/s sec peak velocity was imposed over a  $40^\circ$  region centered at the pole, beginning at 0.3 ms with a half period of 0.7 ms (Eq. 10).

The computational results confirmed the occurrence of coup and contrecoup cavitation and the calculated CSF pressures agree qualitatively with experimental data (Fig. 17). The simulated snap back effect of the coup side sustains a cavitation from 0.5 to 1.2 ms after the acceleration phase, followed by a strong spike reaching 125 psi, in close agreement with data for P2 (Fig. 17). On the contrecoup side, the calculated P4 pressure shows that cavitation occurs at 0.1 ms and collapses at 0.4 ms, followed by some oscillation (Fig. 17a). The recorded P4 pressure confirms the contrecoup cavitation but shows a later collapse at 0.6 ms, followed by some oscillation probably due to structural ringing that was not modelled.

## DISCUSSION

This study investigated the fluid dynamic effects on the loading response of the cranium-brain system using a computational and a physical model. The physical model consists of an idealized cranium with a balloon inserted in it to simulate the brain. Significant peak pressure reduction was observed by introducing just 3.1% volume fraction of air into the brain fluid. The tests with different neck openings showed some sensitivity of loading response to the flow resistance at the foramen magnum.

The fluid response of the brain and CSF under strong acceleration was simulated using an idealized Eulerian computational fluid dynamics model. When the brain is 15% heavier than the CSF, flow velocity from 1-2 ft/s in the CSF layer develops under a translational impact loading, and the brain is estimated to move 3-7% in 12 ms into the subarachnoid CSF layer. With frontal structural deformation, the calculated coup-contrecoup pressures become asymmetric with increased peak magnitudes, in agreement with experimental data. The model reproduces the strong fluid dynamic effects when cavitation occurs as observed in the high acceleration tests. The snap back of the frontal impact site can produce a coup cavitation with a strong pressure spike when the bubbles collapse.

The calculations show that cranial deformation increases the coup-contrecoup pressure peak magnitudes asymmetrically increasing the chance of cavitation. Fluid-structure coupling has been recognized as a significant phenomenon for head impact, and our fluid dynamic results are in agreement with previous investigations (Kenner and Goldsmith, 1973; Merchant and Crispino, 1974). The favourable data comparison confirms that the fluid structure at the CSF-cranium boundary is important in modelling of the brain response to head impact.

The computational fluid dynamics results are consistent with the observation of coup-contrecoup cavitation injury (Hosey et al., 1982). These simulations take the cavitation injury hypothesis to a higher level of detail with the accounting for the thermo-fluid dynamic process. For cavitation response, an Eulerian two-fluid model is more advantageous than a Lagrangian structural approach in simulating the interphase heat and mass transfer and bubble collapse. The Eulerian two-fluid approach is advantageous in modelling strong fluid motion and cavitation effects. A coupled Eulerian-Lagrangian fluid-structure model is needed to simulate realistic brain-cranium interaction with CSF effects. This study provides new fluid dynamics response data useful in understanding the cranium-brain system under impact loading situations. Efforts should also be made to correlate idealized results with realistic injury criteria.

The limitations of the idealized computational model are: 1) the use of a cylindrical approximation does not capture three dimensional effects, 2) no full fluid-structure coupling between the cranium and CSF, and 3) an unclear connection between simulation results and actual brain injury. The simulated significant effects of cranial deformation and acceleration on CSF and brain pressures indicate the need of coupled fluid-structure modelling for brain injury analysis. To provide closer connection between model results and actual injury observation, more realistic three-dimensional computational modelling along with surrogate test modelling work is needed.

## REFERENCES

- CHAN, H. S. AND LIU, Y. K. (1974). "The Asymmetric Response of a Fluid-Filled Spherical Shell-A Mathematical Simulation of a Glancing Blow to the Head," *J. Biomechanics*, Vol. 7, pp. 43-59.
- CHAN, R.K.-C., MASIELLO, P. J. AND SRIKANTIAH, G. S. (1986). "PORTHOS - A Computer Code for Solving General Three-dimensional, Time-Dependent Two-Fluid Equations," ASME Paper 86-WA/NE-3, Winter Annual Meeting, Anaheim, CA.

- CHAN, P. C. AND KLEIN, H. H. (1994). "A Study of Blast Effects Inside an Enclosure," *ASME J. Fluids Engineering*, Vol. 116, pp. 450-455, Sept. 1994.
- CHAN, P. C. AND KLEIN, H. H. (1989). "Computational Studies of Venting Hydrogen Flame Impingement on the Space Shuttle External Tank," AIAA-89-0318, 27th Aerospace Sciences Meeting, Jan. 9-12, 1989.
- DENNY-BROWN, D. AND RUSSELL, W.R. (1941). "Experimental cerebral concussion: Brain", Vol. 64, pp. 93-164.
- ENGIN, A. E. AND LIU, Y. K. (1970). "Axisymmetric Response of a Fluid-Filled Spherical Shell in Free Vibrations," *J. Biomechanics*, Vol. 3, pp. 11-12.
- HOSEY, R.R. AND LIU, Y.K. (1982). "A Homeomorphic Finite Element Model of the Human Head and Neck, in "Finite Elements in Biomechanics, R. H. Gallagher et al (Ed.), John Wiley & Sons, Ltd.
- KLEIN, H.H., CHAN, P.C., AND CHAN, R.K.-C. (1989). "CFD Analysis of the Hydrogen Disposal System at the Vandenberg Space Shuttle Launch Site," AIAA-89-0579, 27th Aerospace Sciences Meeting, Reno, Nevada, Jan. 9-12, 1989.
- KENNER, V.H. AND GOLDSMITH, W. (1973). "Impact on a simple physical model of the head" *J. Biomechanics*, Vol., 6, pp. 1-11.
- KOPECKY, J.A. AND RIPPERGER, E.A. (1969). "Closed Brain Injuries: An Engineering Analysis," *J. Biomechanics*, Vol. 2, pp. 29-34.
- LILES, D.R. AND REED, W.H. (1978). "A Semi-Implicit Method for Two-Phase Fluid Dynamics," *J. Computational Physics*, Vol. 26, No. 3, pp. 390-407.
- LJUNG, C. (1975). "A Model for Brain Deformation Due to Rotation of the Skull," *J. Biomechanics*, Vol. 8, pp. 263-274.
- MCELHANEY, J. H., MELVIN, J. W., ROBERTS, V. L. AND PORTNOY, H. D. (1973). "Dynamic Characteristics of the Tissues of the Head," in Perspectives in Biomedical Engineering, Kenedi, R. M. (Ed.), MacMillan Press, London, pp. 215-222.
- MERCHANT H.C. AND CRISPINO, A.J. (1974). "A Dynamic Analysis of An Elastic Model of the Human Head," *J. Biomechanics*, Vol. 7, pp. 295-301.
- MOHAN, D., BOWMAN, B.M., SNYDER, R.G. AND FOUST, D.R. (1979). "A Biomechanical Analysis of Head Injury to Children," *Trans. of the ASME*, Vol. 101, pp. 250-260.
- STALHAMMAR, D.A., (1970). "The Mechanism of Brain Injuries," in Handbook of Clinical Neurology: Head Injury, Vinken, et al. (Ed.), Elsevier Science Publishers.
- UNTERHARNSCHEIDT, F.J. AND RIPPERGER, E.A. (1970). "Mechanics and Pathomorphology of Impact-Related Closed Brain Injuries," in Dynamic Response of Biomechanical Systems, ASME Winter Annual Meeting, NY, Dec. 2, pp. 46-83.
- TALHOUNI, O. AND DIMAGGINO F. (1975). "Dynamic Response of a Fluid-Filled Spheroidal Shell-An Improved Model for Studying Head Injury," *J. Biomechanics*, Vol. 8, pp. 219-228.
- VIANO, D.C., KING, A.I., MELVIN, J.W. AND WEBER, K. (1989). "Injury biomechanics research: An essential element in the prevention of trauma," *J. Biomechanics*, Vol. 22, No. 5, pp. 403-417.
- WARD, C. (1983). "Finite Element Modelling of the Head and Neck," in Impact Injury on the Head and Spine, Ewing C. et al. (Ed.), Charles Thomas, Ch. 14, pp. 421-474.

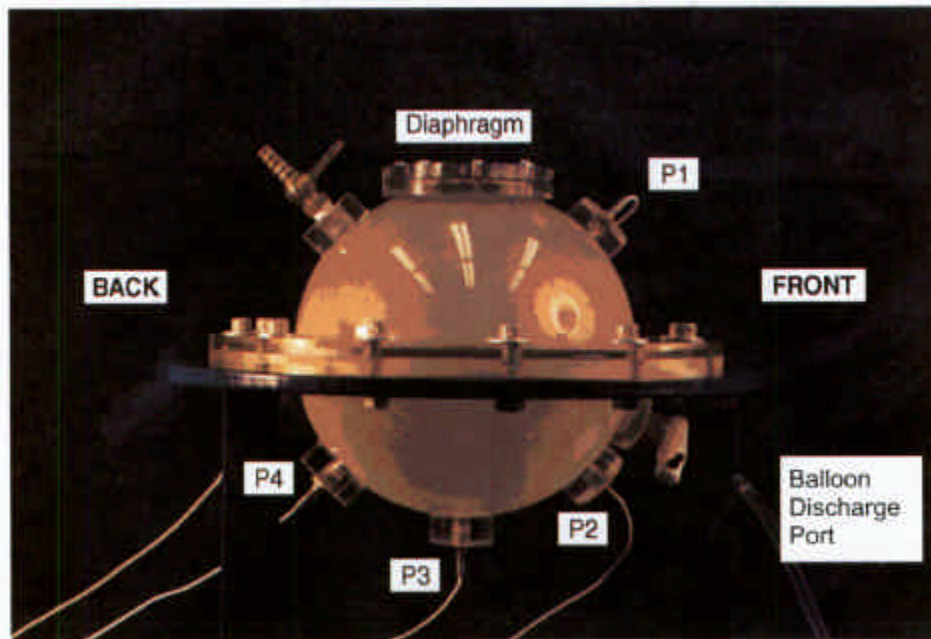


Figure 1. Photograph of Cranium-CSF-Brain physical model showing the diaphragm where load is applied to the fixed model. Pendulum impact load is applied at the equatorial flange of the free-hanging model. Front and Back correspond to coup and contrecoup.

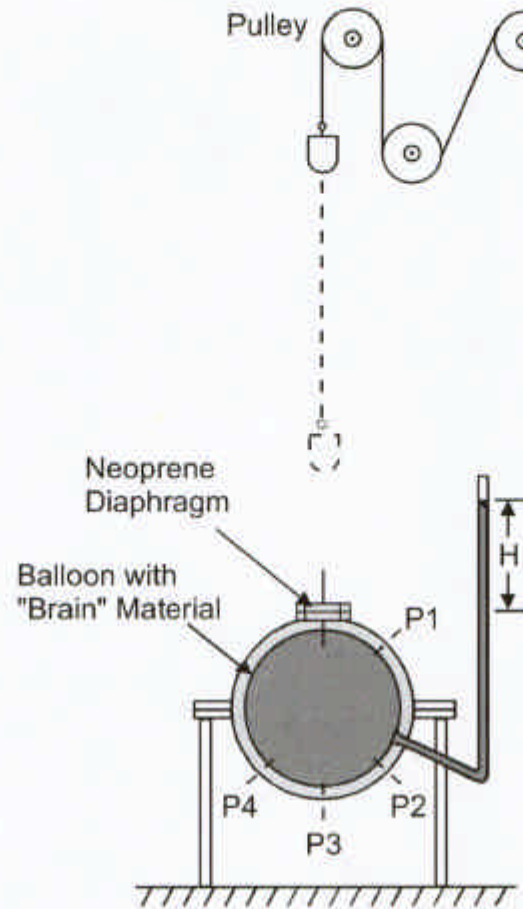


Figure 2. Schematic diagram of deformation-impact test. Load is applied to the fixed model by controlled weight drop on the top diaphragm. Foramen magnum flow is allowed through a discharge port that is controlled by water column H.

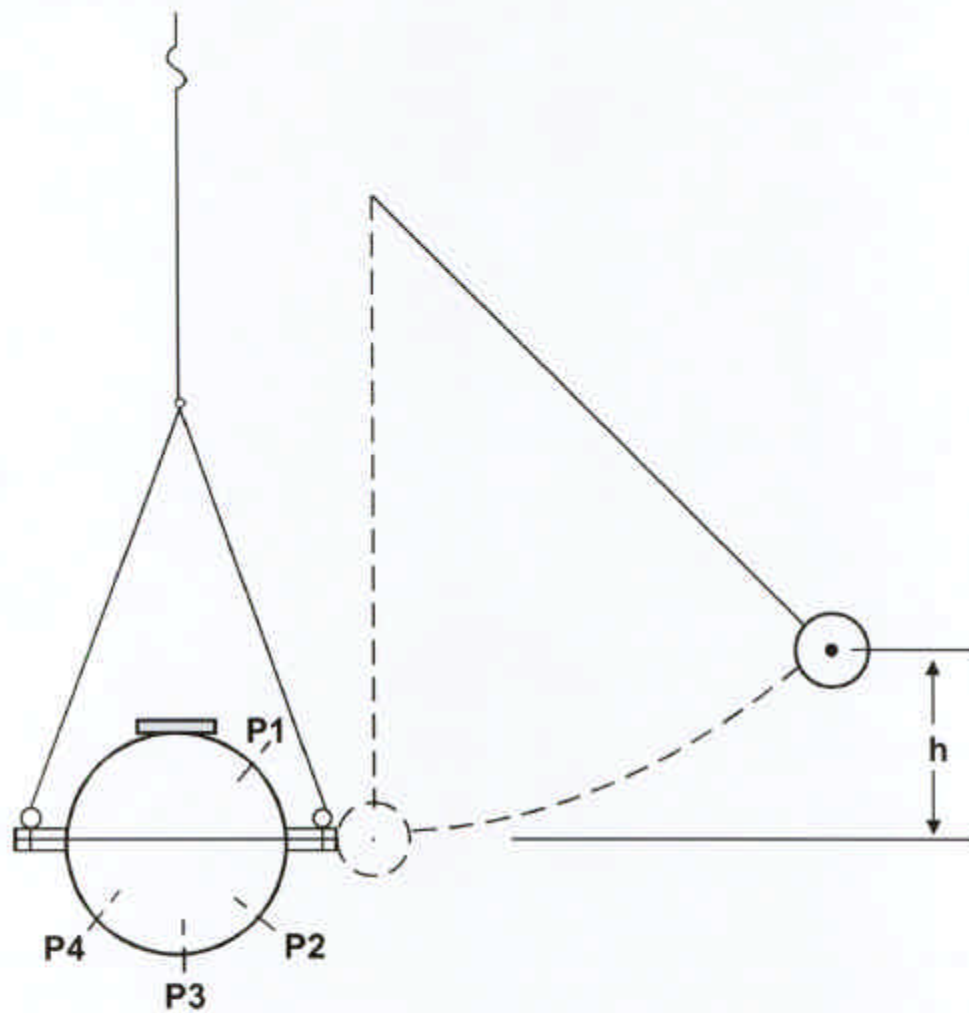


Figure 3. Schematic diagram of pendulum impact test. Load is applied to the free-hanging model by free-swinging pendulum weight with controlled initial height,  $h$ .

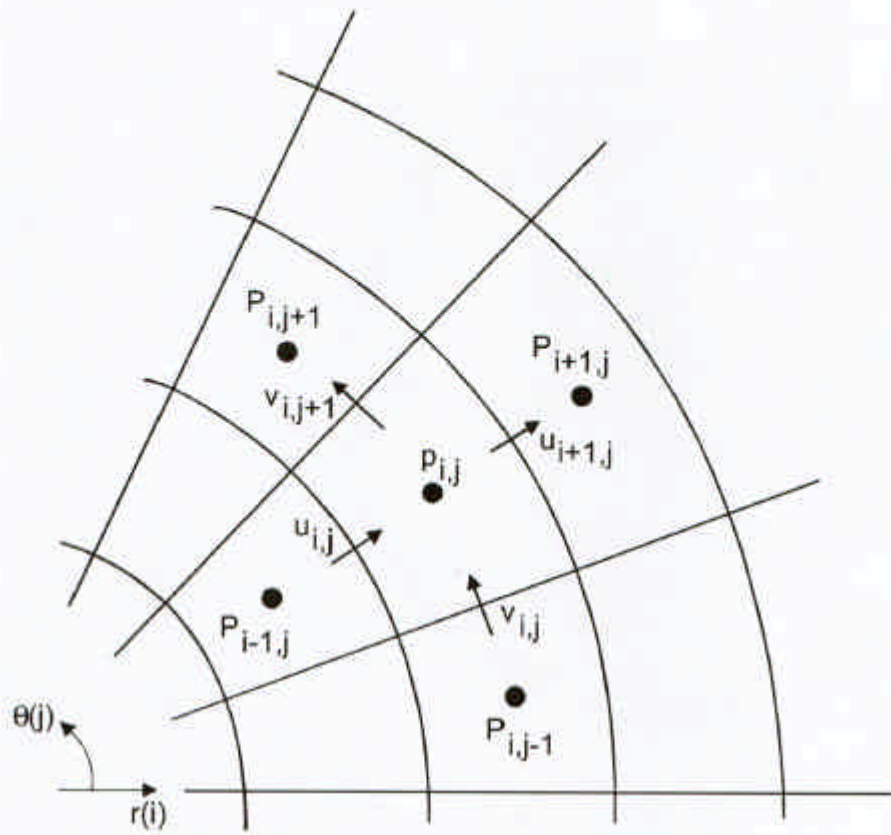


Figure 4. Staggered computational mesh system for computational fluid dynamics calculations in planar cylindrical coordinates,  $(r - \theta)$ . Pressure (scalar) is at cell center with velocities at cell edges.

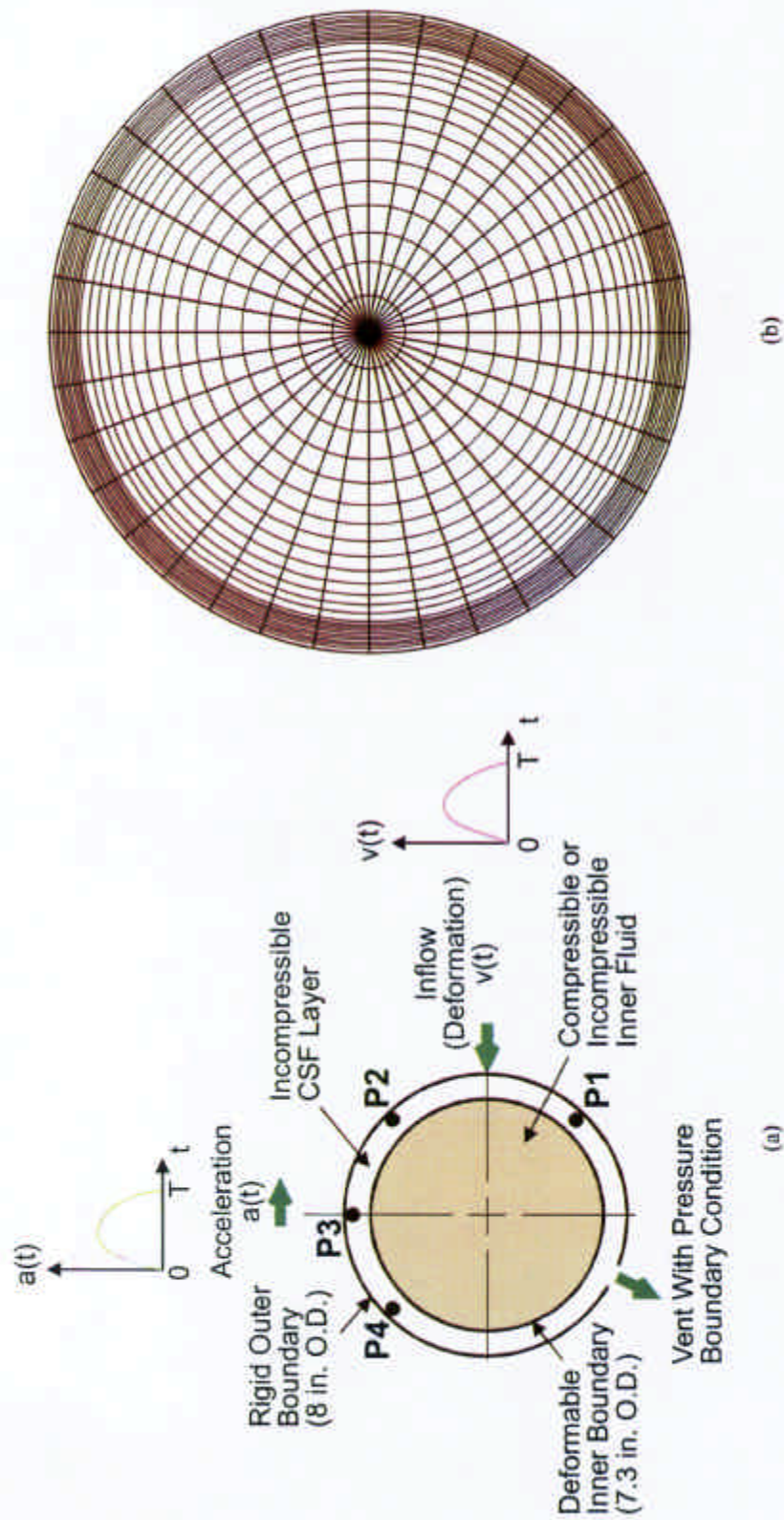


Figure 5. (a) Schematic diagram of the planar cylindrical Cranium-CSF-Brain model (b) Computational model using planar cylindrical computational mesh with fine mesh placed between the cranium and the brain to resolve CFS flow field.

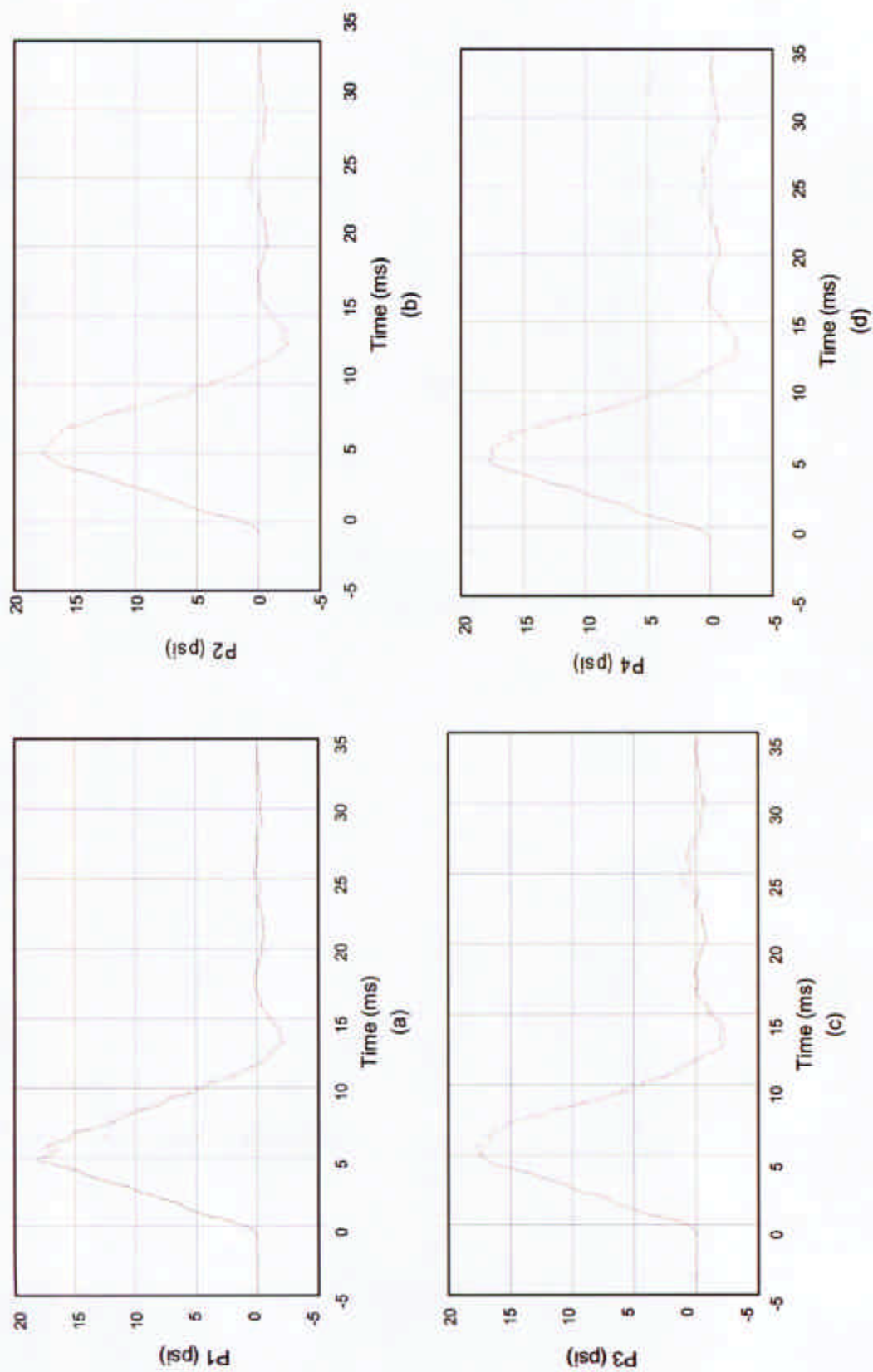


Figure 6. Repeatability tests showing pressure responses with balloon discharge port closed and both balloon and CSF layer filled with water. Deformation was applied to top diaphragm by controlled weight drop with test repeated 4 times. (a) Gauge P1 (45°), (b) Gauge P2 (135°), (c) Gauge P3 (180°, mid-plane), (d) Gauge P4 (225°)

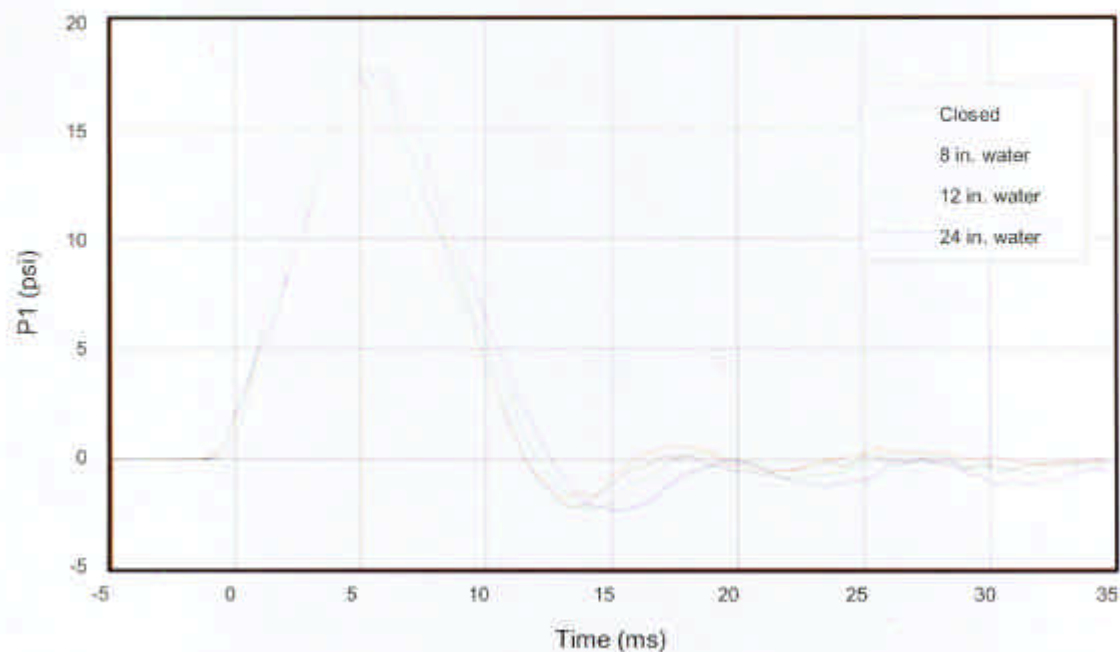


Figure 7. Effect of foramen magnum flow resistance on pressure at P1. Balloon discharge port resistance was controlled by water column at 8, 12 and 24 inch height.

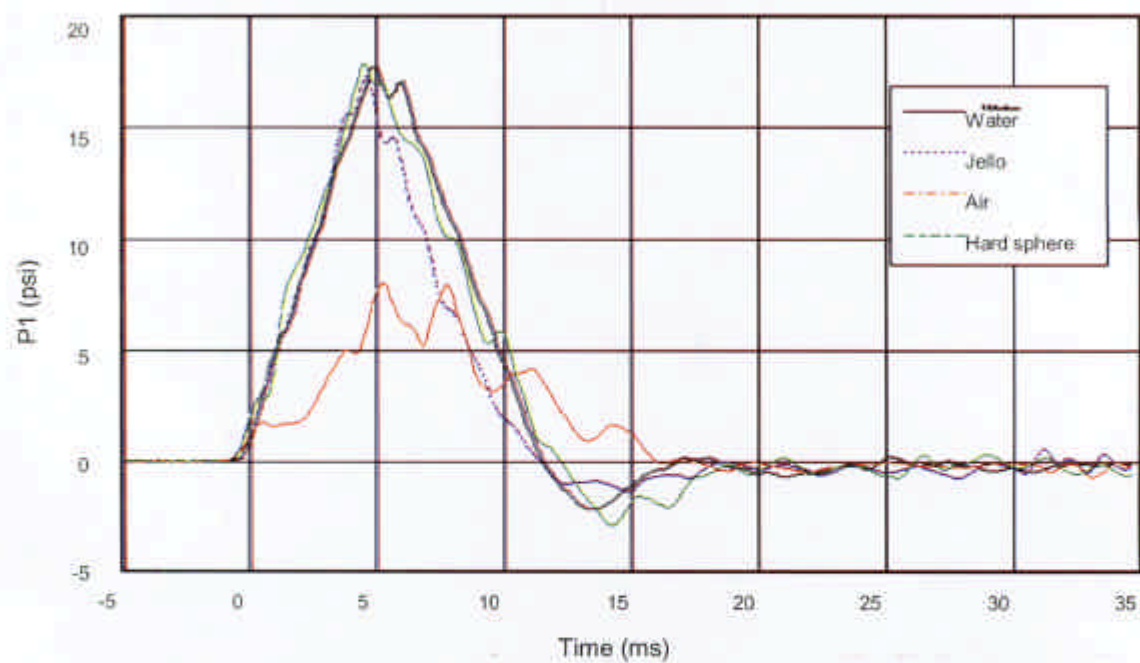


Figure 8. Effect of brain simulant material differences on pressure at P1. Significant effect observed when compressibility was introduced by inserting a 3.1% air bubble (balloon) into the brain simulant.

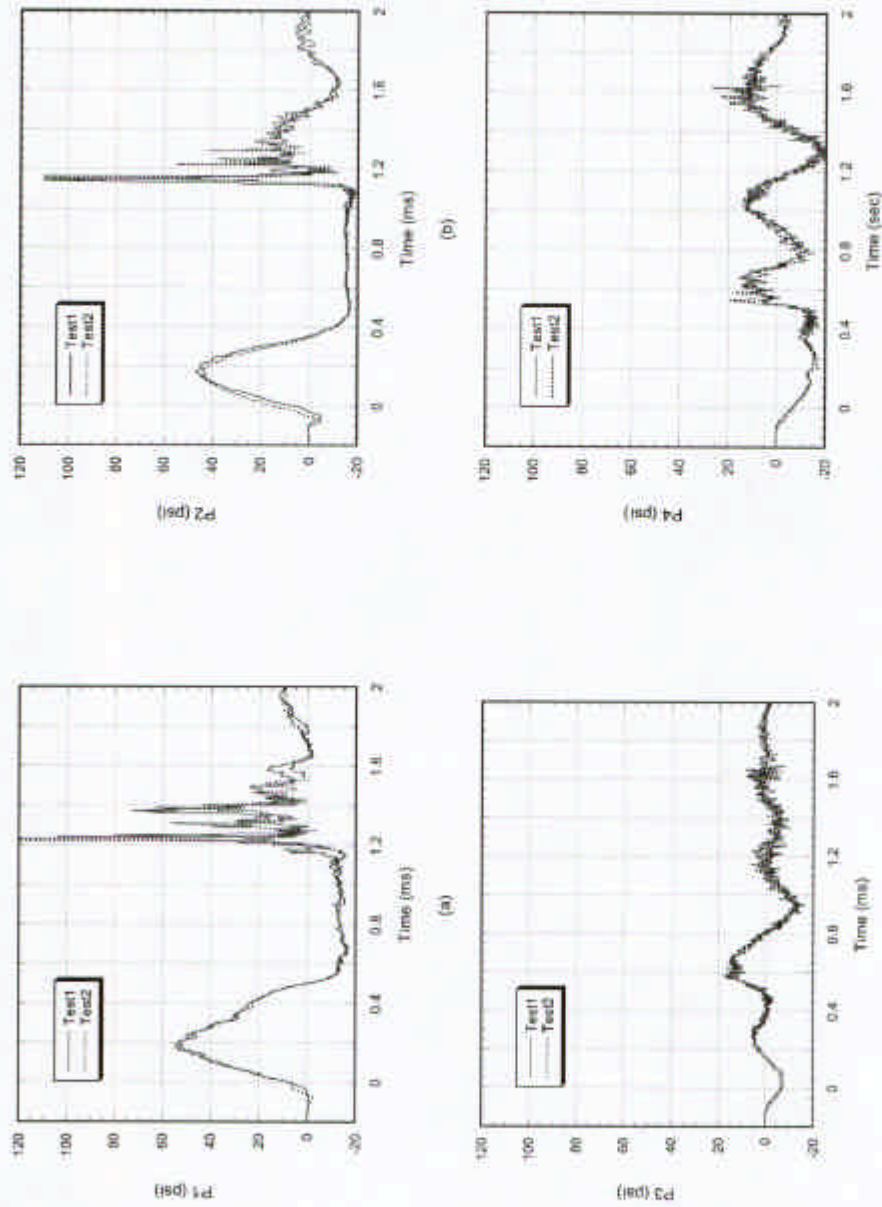
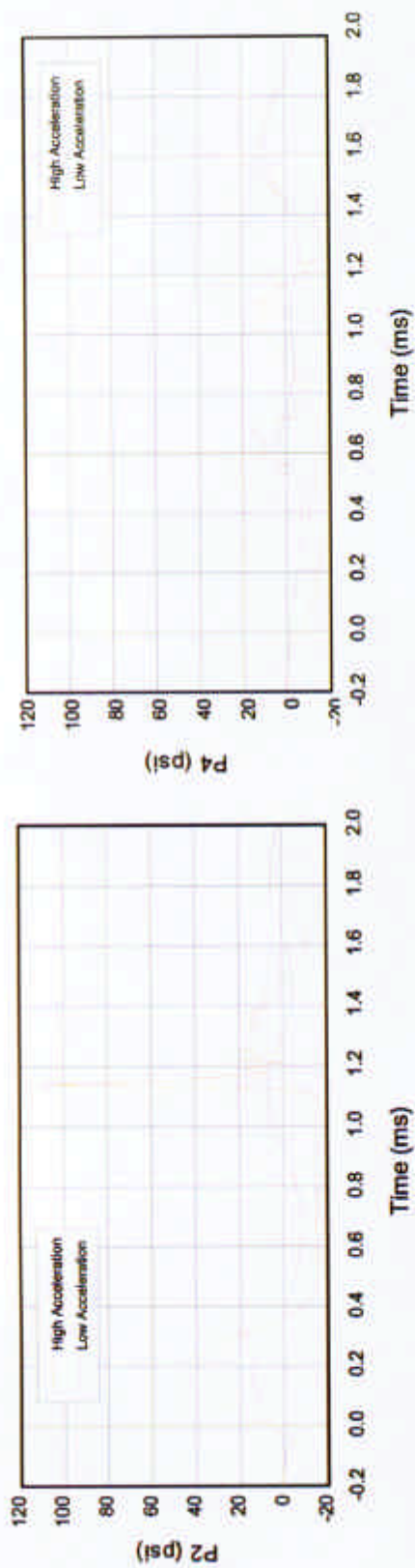


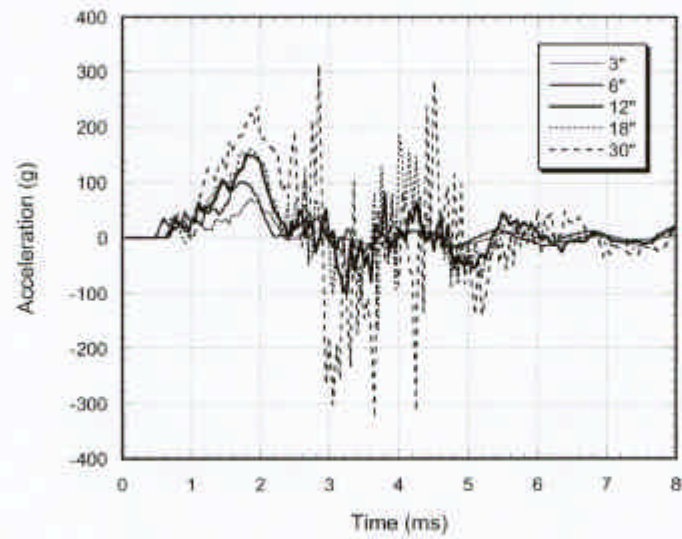
Figure 9: Repeatability tests for the pendulum-loaded free hanging model under loading strong enough to cause coup and contrecoup cavitation. (a), (b) Coup cavitation resulting from snap back of structural indentation, with pressure spike near 1.2 ms caused by cavitation bubble collapse. (c) Mid-plane pressure (d) Contrecoup cavitation (P4) was due to acceleration effect with bubble collapse observed around 0.5 ms.



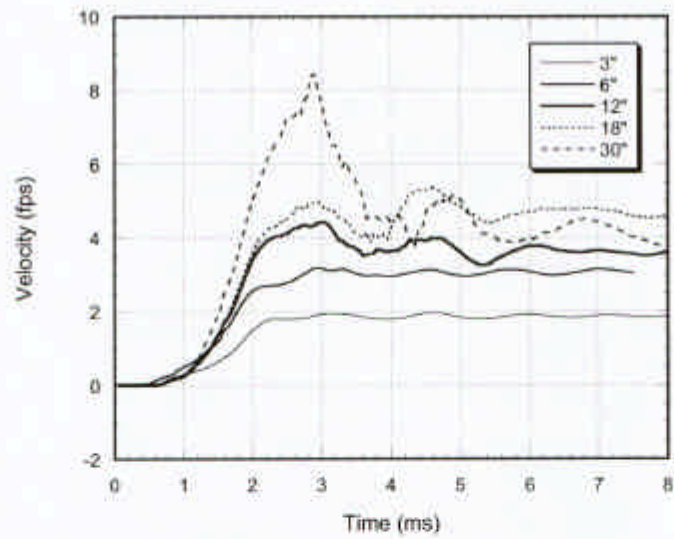
(a)

(b)

Figure 10. Comparison of pressure responses between high and low acceleration impacts. High acceleration caused cavitation due to structural snap back on (a) the coup side and acceleration effects on (b) the contrecoup side. No cavitation was produced by the low acceleration impact.

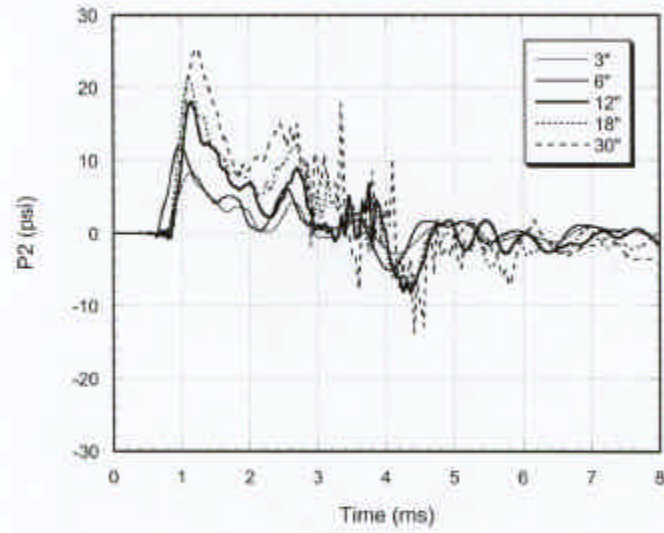


(a)

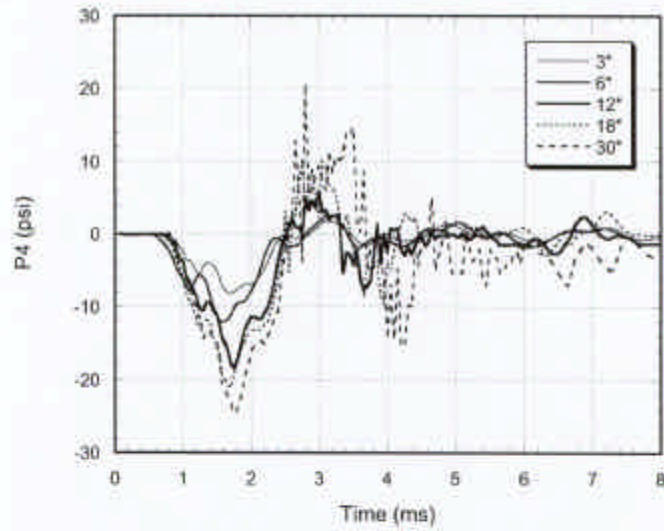


(b)

Figure 11: (a) Acceleration of free hanging model with impact applied to the delrin-reinforced equatorial flange by the pendulum at various heights. (b) Model velocity integrated from acceleration.



(a)



(b)

Figure 12: Effects of acceleration on coup and contrecoup pressures for test conditions shown in Fig. 11.  
(a) no cavitation, (b) contrecoup cavitation at pendulum height of 30" occurs at around 2.7 ms.

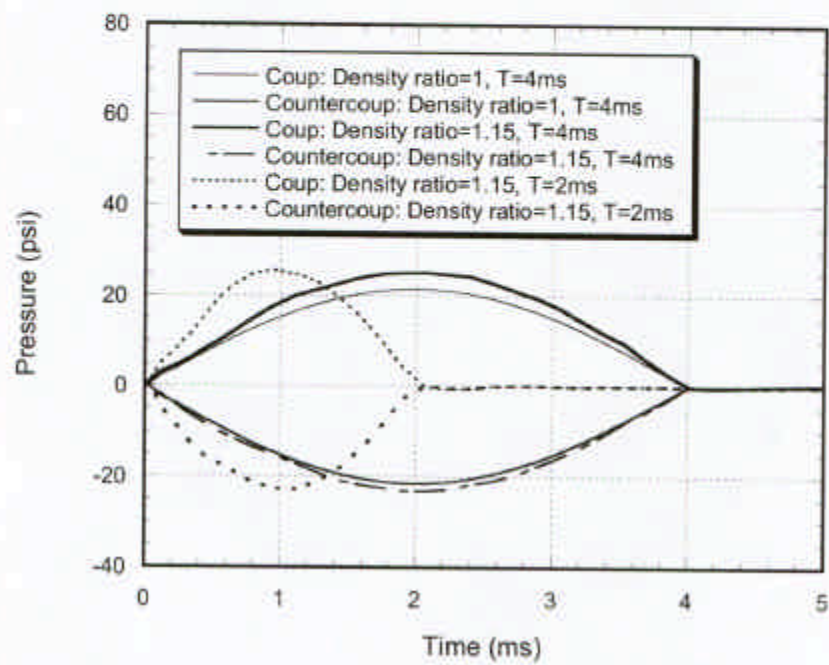


Figure 13: Effects of brain-CSF density ratio on coup and contrecoup pressures under acceleration loading.

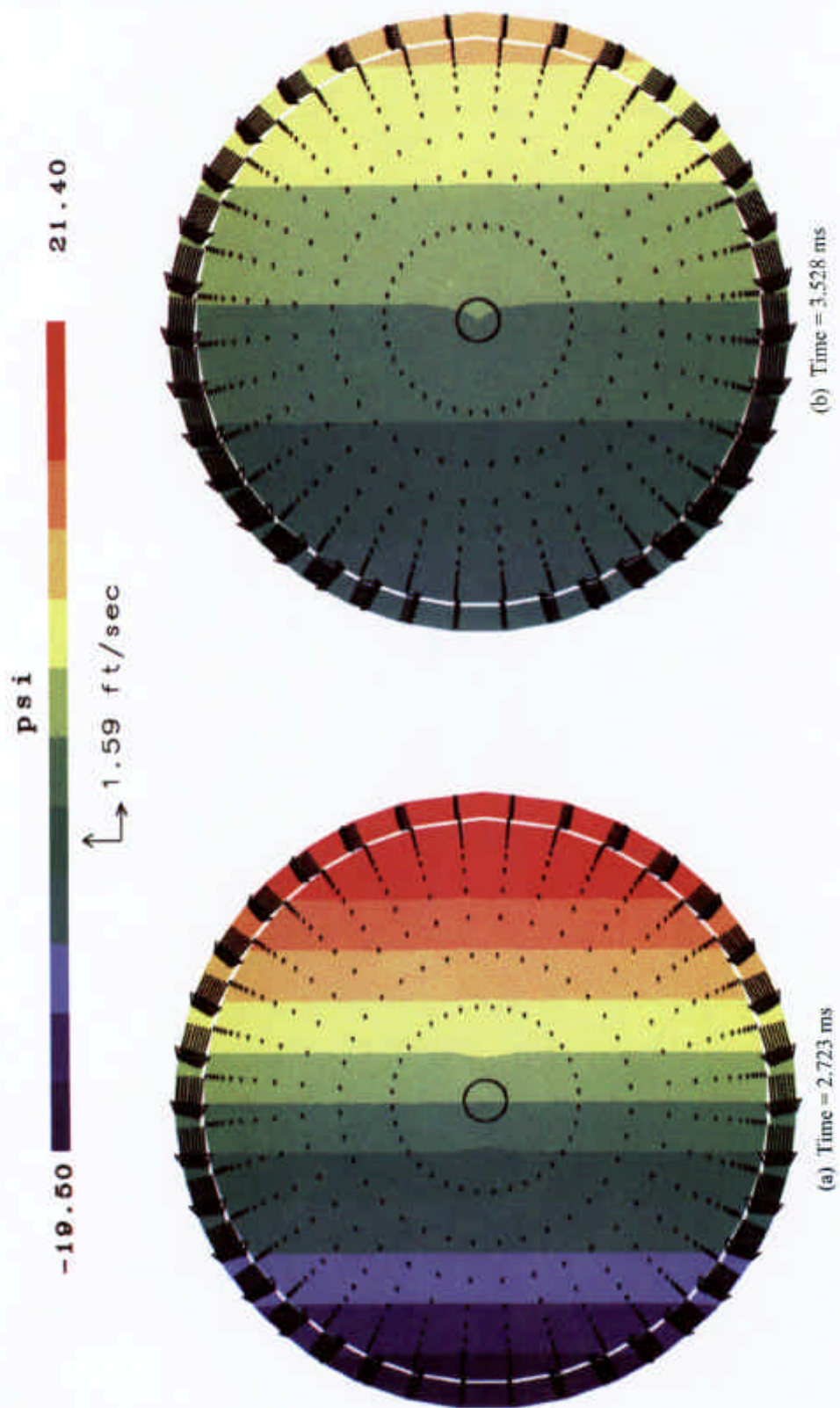


Figure 14: Calculated CSF and brain fluid flow motion with the brain-CSF density ratio of 1.15 and acceleration pulse duration of 4 ms.

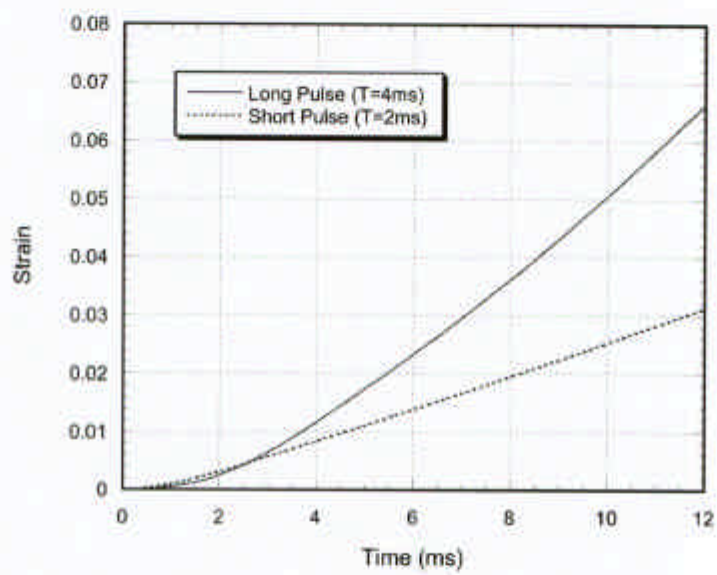
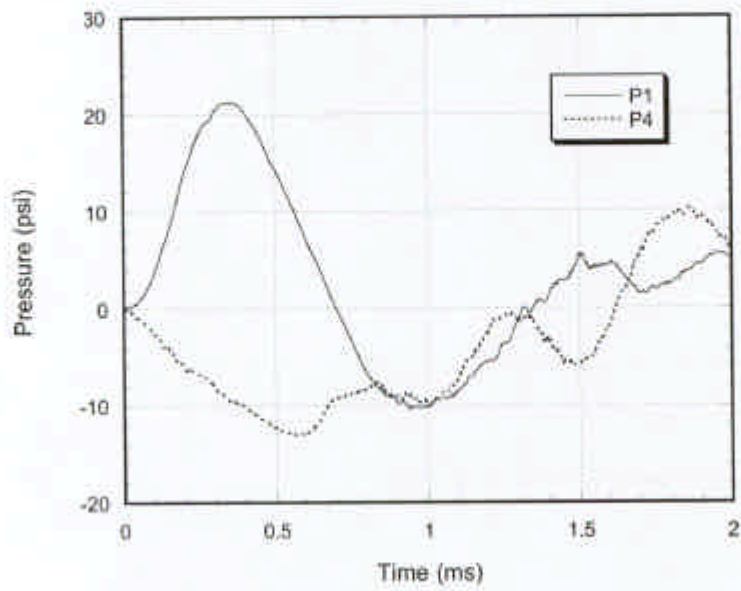
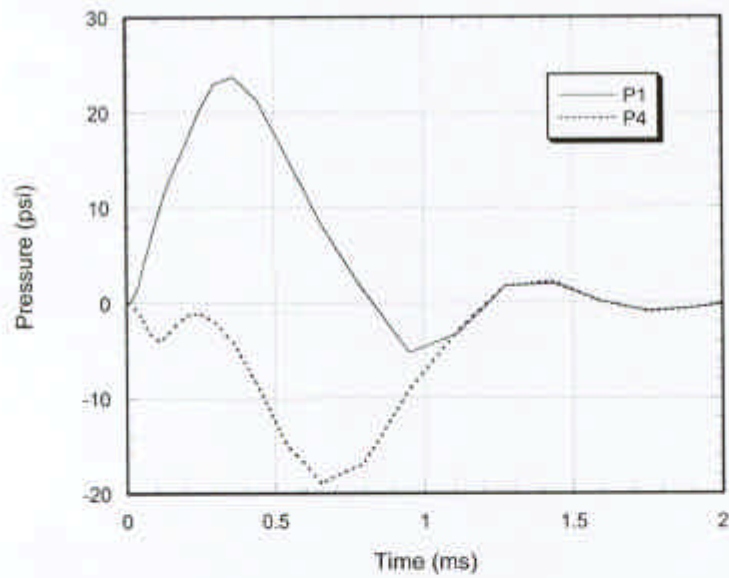


Figure 15: Normalized relative brain displacement expressed as 1-D strain, due to acceleration effects with brain-CSF density ratio of 1.15 corresponding to Fig. 13.

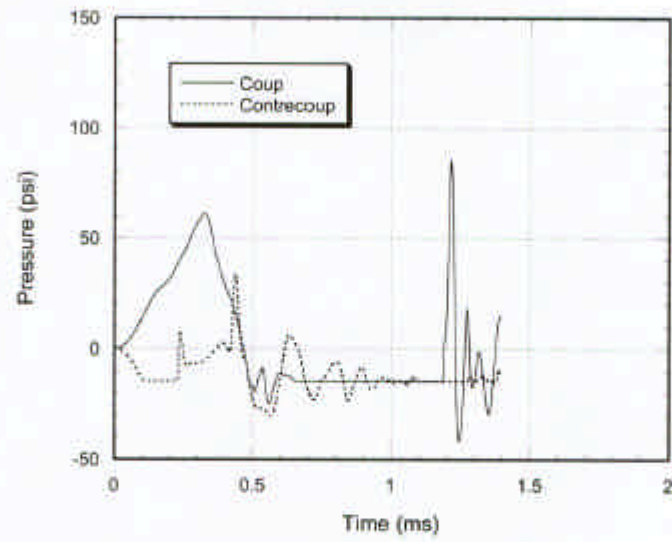


(a)

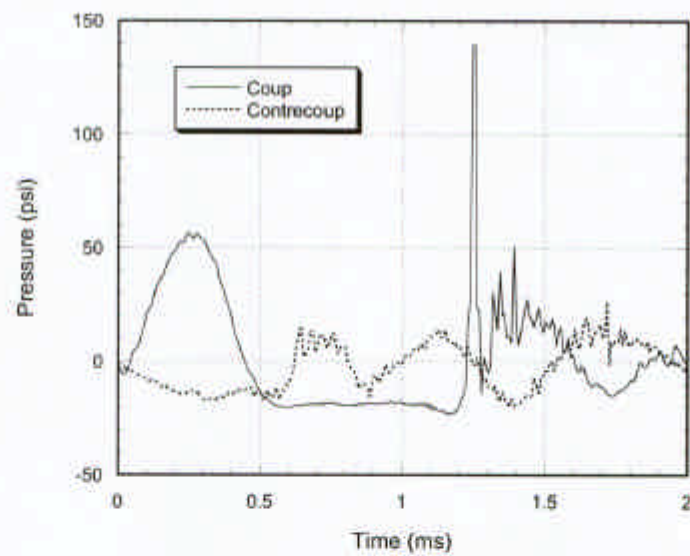


(b)

Figure 16: Effects of acceleration and deformation on coup (P1) and contrecoup (P2) pressures for the non-cavitation case with both the brain and CSF simulated as water with foramen magnum closed; (a) Test data at P1 and P4; (b) Calculated pressures at P1 and P4.



(a)



(b)

Figure 17: Effects of acceleration and deformation on coup and contrecoup pressures, cavitation case with the brain and CSF simulated as water with the foramen magnum opening closed. (a) calculation, (b) test data.